Ternary Gas Mixture Separation in Two-Membrane Permeators

Single-stage separation of ternary gas mixtures of He, CO_2, and N_2 in a hollow-fiber permeator that simultaneously houses two different types of membranes, cellulose acetate and silicone rubber, was investigated. The two membranes have reverse selectivities with respect to He and CO_2. Such a two-membrane permeator separates the feed into three streams, two permeates and one reject, each stream being enriched in a different component. The species permeabilities through each membrane were measured independently, and these values were utilized in a simulation that incorporates the fiber lumen pressure drops, the elastic deformation of the silicone capillaries, and the asymmetric structure of the CA membrane. Simulation results are compared with experimental data. Effects of flow pattern, relative permeation areas of the two membranes, permeate pressure ratios, feed composition, and membrane selectivities are studied. Advantages of the two-membrane scheme over the conventional permeators with only one kind of membrane are discussed.

A. Sengupta and K. K. Sirkar
Department of Chemistry and Chemical Engineering
Stevens Institute of Technology
Castle Point, Hoboken, NJ 07030

Introduction

Membrane gas separation has become a technology of considerable interest over the last two decades. The process works on the principle of selective permeation through a membrane. Conventionally, the separation is achieved by a membrane in a permeator where the faster permeating component is separated from the slower permeating component. Consequently, such permeators can achieve only binary separations. In many processes, however, gas mixtures have more than two components, and separate recoveries of two of the faster components may be desirable in some situations. The concept of two-membrane permeators has been suggested for such cases (Sirkar, 1980).

Figure 1 represents schematically one such permeator. Here the permeator houses two different types of membranes, *A* and *B*. A ternary feed containing three species, 1, 2, and 3 is introduced to this permeator such that the feed is exposed simultaneously to the two membranes. Let the species-membrane combination be such that membrane *A* is more selective to component 1 than the other two species, and membrane *B* is more selective to component 2 than the other two species. In this separation scheme one can therefore recover two separate permeate streams, one enriched in species 1, the other enriched in species 2. At the same time, the unpermeated (reject) stream will be enriched in species 3, the slowest permeating species. A single module can thus bring about a ternary separation. The primary requirement in such a separation scheme is that the two membranes *A* and *B* must have so-called reverse selectivities. This means that component 1 must be more permeable than component 2 through membrane *A*, while 2 must be more permeable than 1 through *B*.

The two-membrane permeator for gas separation was first introduced by Kimura et al. (1973) and Ohno et al. (1977). These workers and others (Stern et al., 1984; Perrin and Stern, 1985a, b) have investigated such schemes for binary separation. Sirkar (1980) studied the concept theoretically under simplifying conditions for ternary separations and showed its advantages. Sengupta and Sirkar (1984) numerically modeled ternary separation in two-membrane permeation separation schemes for the case of homogeneous membranes, and carried out a parametric analysis under the situation of no pressure drop in the bulk flow directions.

The purpose of the present investigation is to study ternary gas separation in two-membrane permeators experimentally, and to make a comprehensive and realistic simulation of the separation process. Selection of a gas mixture for study was one of the very first steps. Table 1 lists some relevant multicomponent gas mixtures of interest. An inspection of the list suggests that a mixture of H_2—CO_2—N_2 may best represent the scope of this kind of separation scheme, the objective of separation being sep-

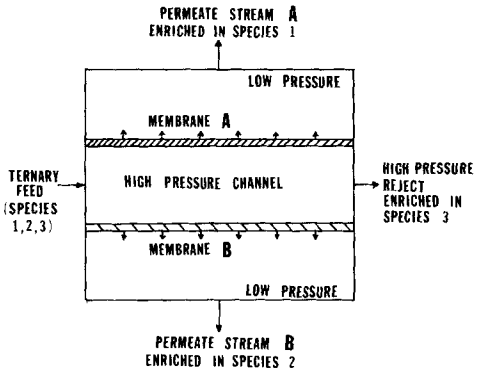

Figure 1. Two-membrane permeator configuration.

arate recovery/enrichment of H_2 and CO_2. Although many of the mixtures shown contain CO, it can be considered to be the same as N_2, since N_2 and CO have very similar permeation properties through most polymeric membranes. Besides, in actual experiments H_2 was replaced by He for safety reasons. These two gases usually have similar permeabilities. A composition range of 30–50% He, 10–15% CO_2, and balance N_2 was considered suitable for investigation.

Selection of a pair of membranes was the next step. One is necessarily restricted here by the availability of membranes. About the only two available polymeric membranes that satisfied the criterion of reverse selectivity were cellulose acetate (CA) hollow fibers and silicone (S) rubber capillaries. CA, which is a glassy polymer, is more permeable to He than it is to CO_2, and the hollow fiber has a dense skin on the outside supported by an integral microporous backing (Pan, 1983). Silicone rubber, on the other hand, is more selective to CO_2 than it is to He, and the capillaries are homogeneous and isotropic (Blaisdell and Kammermeyer, 1973; Thorman and Hwang, 1978; Stern et al., 1977).

The above two membranes were potted together inside a shell with the ends separated from each other to individually collect each permeate. In the separation experiments the two following gas compositions were used: 48.6% He–10.1% CO_2–balance N_2, and 31.6% He–13.7% CO_2–balance N_2. The permeates were withdrawn at atmospheric pressure. In most of the experiments the feed pressure was chosen such that the permeate/feed pressure ratios at the permeate outlets were 0.2. Some experiments were carried out at higher feed pressure with the permeate pressure ratios equal to 0.1, but the silicone rubber capillaries were severely compressed at this pressure, and separations were drastically reduced.

The pure-component permeability of each species through each membrane was measured experimentally. These values

Table 1. Some Important Multicomponent Gas Mixtures

Reformed natural gas	H_2—CO_2—CO—CH_4—N_2
Producer gas	H_2—CO_2—CO—N_2
Reformer off-gas	H_2—CO—CO_2
High-sulphur sour natural gas	CH_4—CO_2—H_2S
Post-shift reactor gas	H_2—CO—CO_2—N_2
Ammonia purge stream	H_2—N_2—CH_4—Ar
Natural gas containing He and N_2	He—CH_4—N_2
Deep sea diving gas	He—O_2—N_2

were subsequently used in simulations. The model developed for the simulation incorporated the pressure buildups inside the fiber lumens, and the elastic deformation of the silicone rubber capillaries under pressure (Stern et al., 1977). The CA fibers were supposedly asymmetric in structure (Pan, 1983). The effect of choosing the right model for this structural asymmetry has been studied. Simulation and experimental results have been compared under various parametric conditions. The effect of different flow patterns, membrane area ratio, permeate pressure ratio, and membrane selectivity on the permeator performance have been discussed. The advantages of the two-membrane scheme over a single-membrane permeator are also considered.

Experimental Procedures

The silicone rubber capillaries used were Silastic medical grade tubing made by Dow Corning Corp., Midland, MI. The gas-separating CA fibers were not available directly, however. For this reason, some CA fibers from a Dow reverse-osmosis module (Module No. 96-05, Permutit Co., Paramus, NJ) were solvent-treated and dried as suggested by MacDonald and Pan (1974). Details of the actual method employed are given by Sengupta (1985). After the two sets of fibers were available, they were potted inside a red brass pipe of 2.13 cm OD and 1.59 cm ID. The potting arrangement is shown in Figure 2; the potting process is described thoroughly by Sengupta (1985). Two such permeators were built; the details are provided in Table 2. The potting consisted of one thick epoxy layer sandwiched between two thin layers of silicone rubber. The feed was introduced to and taken out from the shell as shown in Figure 2. The two permeate streams were withdrawn separately from the two permeate headers. By reversing feed in/out directions, one could have either a cocurrent or countercurrent flow pattern vis-a-vis feed and permeates. These were the only two important flow patterns that were utilized in the hollow-fiber permeators. The permeate pressure buildup in the closed ends of the two types of fibers was indicated by the two pressure gauges (Matheson Co., East Rutherford, NJ) on one side of the permeator, Figure 2.

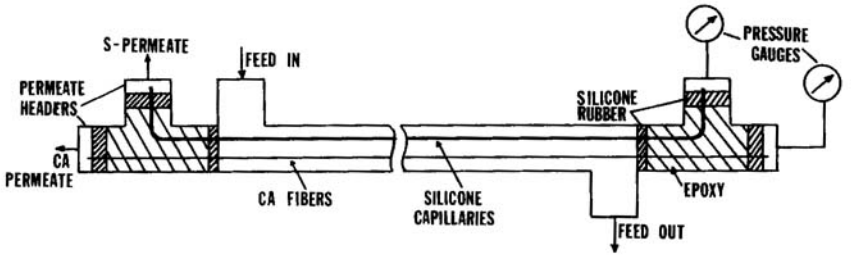

Figure 2. Potting and fiber arrangements in two-membrane permeator.

Table 2. The Permeators

	Permeator	
	No. 1	No. 2
Total no. CA fibers	112	56
Total no. S capillaries	57	57
Eff. permeation length, m	0.50165	0.51435
Total CA membrane permeation area, cm^2	406	208
Total S membrane permeation area, cm^2	404	414.5
Potted length CA membrane, m	0.092	0.090
Potted length S membrane, m	0.091	0.088
Fiber dimensions, μm	ID	OD
CA	84	230
S*	305	635

*Values in unstressed condition; Young's modulus for silicone rubber = 3.088×10^6 Pa (448 psi)

Permeation and separation experiments were carried out in the setup represented schematically in Figure 3. All the flow lines were 0.635 cm (¼ in.) in size. The permeator was immersed in a constant-temperature circulating bath. A feed of known composition was introduced at a controlled flow rate into the permeator shell. The feed pressure was adjusted by a back-pressure regulator on the reject line. The feed could be obtained from a single ternary gas mixture cylinder. Alternatively, the composition could be made up by mixing two gas streams (pure gases or mixtures) using two modular Dyna Blenders (Matheson, model 8250). The feed line consisted of a flow transducer, a flow controller, a gate valve, an oil-moisture trap, and a particulate solids filter. Each of the three outlet lines from the permeator had a pressure gauge (Matheson), a flow transducer (Matheson, model 8141), a back-pressure regulator (Fairchild Co., Salem, NC), and a check valve (C-series, Nupro Co., Willoughby, OH). Using two four-way switching valves (Whitey Co., Highland Heights, OH), the required sample was directed to a Varian 1420 gas chromatograph with a CTR column (Alltech Associates, Deerfield, Il) and a thermal conductivity detector connected to a strip chart recorder.

In pure-component permeation experiments, a feed of the pure gas under consideration was fed to the permeator; the reject line outlet from the permeator was plugged just after the pressure gauge. Only the flow rates of the two permeate streams were measured. A separation experiment, however, involved measuring the flow rates and determining the compositions of the two permeates and the reject. The flow rate, the composition, and the pressure of the feed were known, and so were the permeate outlet pressures. One could vary the feed flow rate, keeping the feed composition and the feed pressure constant, to generate a series of separation data. The process was repeated for different values of feed pressure and/or feed composition. In all the experiments, the permeate pressures at the closed fiber ends were recorded.

Simulation

A number of analyses and simulations are available for single-membrane hollow-fiber permeators with binary systems. Chern et al. (1985) have carried out a rather comprehensive modeling of hollow-fiber permeators. Some of the relevant earlier analyses were done by Antonson et al. (1977), Pan and Habgood (1978), Stern et al. (1977), and Thorman and Hwang (1978). Perrin and Stern (1985a, b) have considered two-membrane permeators for binary separations, and Sengupta and Sirkar (1984) carried out a parametric analysis for ternary separation.

Some of the important points for the present analysis are as follows:

• There are three flow streams at any cross section of the permeator. Each of these streams is a ternary mixture; thus the concentrations of at least two components need to be specified in order to identify the mixture composition.

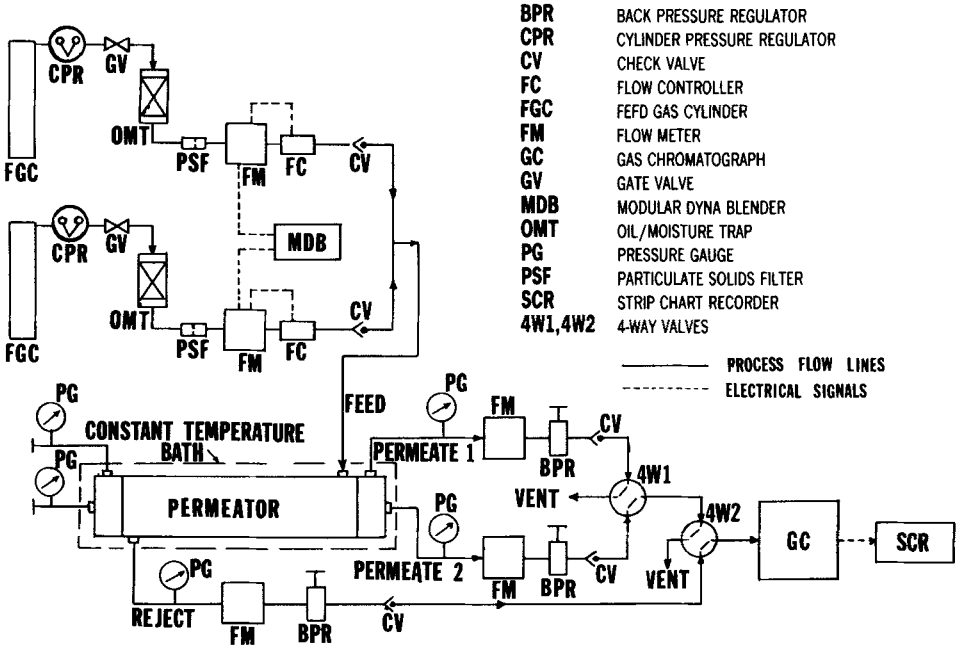

Figure 3. Experimental setup.

• The flow rate, the composition, and the pressure of each stream is likely to change along the length of the permeator.

• The feed/permeate flow pattern inside the permeator is important in the theoretical formulation.

One has also to consider the effect of the membrane structure and the elastic deformation of the fibers, if any.

The basic assumptions in the present modeling are:

1. The feed (shell) side of the permeator has no pressure drop.
2. End effects inside the permeator are negligible.
3. There is negligible gas phase mass transfer resistance in the direction of permeation, and no axial dispersion in the bulk flow directions.
4. The permeability of a species does not change appreciably with its partial pressure, or because of the presence of other species, under the experimental conditions.
5. Poiseuille flow can be assumed inside the CA fibers.
6. CA fibers act as rigid capillaries with no deformation.
7. The deformation of the silicone rubber capillaries can be modeled on the basis of large deflection analysis of thick-walled isotropic incompressible elastic tubes as developed by Stern et al. (1977).
8. The viscosity of a gas mixture is independent of the partial pressure of the species, but depends on the composition of the mixture.

To formulate the balance equations, the permeator is represented in the form shown in Figure 4. This figure shows the countercurrent flow pattern only. The situation will be almost identical for cocurrent flow, with only a change in the flow direction of the feed. As shown, x_1 and x_2 represent the local mole fractions of components 1 and 2, respectively, in the feed channel. Of the two subscripts in the permeate mole fraction, represented by y_{ij}, the first designates the membrane number, and the second the species number. The permeability coefficient Q_{ij} similarly has two subscripts. For other symbols, refer to the Notation.

Assuming for the time being that the CA fibers are asymmetric, with the active skin on the outside, a differential material balance on component j in the CA permeate (assumed to be permeate stream number 1) yields

$$d(V_1 y_{1j}) = \pi D_{OCA} dl N_{TCA} (Q/d)_{1j} (P_f x_j - p_1 y'_{1j}) \qquad (1)$$

The term (Q/d), called here the specific permeability, is used in Eq. 1 since the effective membrane thickness, d, is not known for asymmetric membranes (Stern et al., 1974; Sirkar, 1977; Pan et al., 1978). Also, as Pan (1983) showed, the quantity y'_{ij}, the permeate mole fraction based on cross flow, should be used for an asymmetric membrane instead of y_{ij}, the bulk permeate mole fraction.

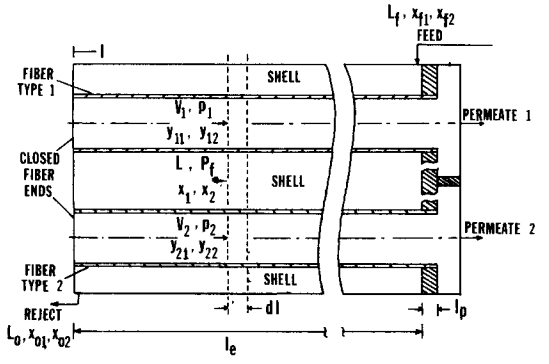

Figure 4. Material balance in two-membrane permeator.

In dimensionless form, Eq. 1 can be written as

$$d(V_1^* y_{1j})/dl^* = KC_{1j}(x_j - \gamma_1 y'_{1j}), \quad j = 1, 2, 3 \qquad (2)$$

where

$$l^* = l/l_e \qquad (3)$$

$$V_i^* = V_i/L_f, \quad i = 1, 2 \qquad (4)$$

$$\gamma_i = p_i/P_f, \quad i = 1, 2 \qquad (5)$$

$$C_{ij} = (Q/d)_{ij} \Big/ \left[\sum_{i=1}^{2}\sum_{j=1}^{3} (Q/d)_{ij}\right] \qquad (6)$$

$$K = \pi D_{OCA} l_e N_{TCA} \left[\sum_{i=1}^{2}\sum_{j=1}^{3} (Q/d)_{ij}\right] P_f/L_f \qquad (7)$$

One can write Eq. 2 for $j = 1$, 2, and 3, and add up to get

$$dV_1^*/dl^* = K(B_1 - \gamma_1 E_1) \qquad (8)$$

where

$$B_1 = C_{11}x_1 + C_{12}x_2 + C_{13}x_3 = C_{13} + (C_{11} - C_{13})x_1 + (C_{12} - C_{13})x_2 \qquad (9)$$

$$E_1 = C_{11}y'_{11} + C_{12}y'_{12} + C_{13}y'_{13} = C_{13} + (C_{11} - C_{13})y'_{11} + (C_{12} - C_{13})y'_{12} \qquad (10)$$

The quantities y'_{11} and y'_{12} are obtained from the following expression (Sengupta and Sirkar, 1984):

$$y'_{1j} = [d(V_1^* y_{1j})/dl^*]/(dV_1^*/dl^*), \quad j = 1, 2 \qquad (11)$$

The material balance in the permeate through the silicone rubber membrane (membrane 2) is somewhat different since the dimensions of the silicone rubber capillaries change upon the application of external pressure. It can be shown that a material balance on component j in permeate 2 is (Sengupta, 1985):

$$d(V_2 y_{2j}) = g\pi D_{lmS} dl N_{TS} (Q/d)_{2j} [P_f x_j - p_2 y_{2j}] \qquad (12)$$

where

$$g = \ln (r_O/r_I)/\ln (R_O/R_I) \qquad (13)$$

and

$$D_{lmS} = 2(r_O - r_I)/\ln (r_O/r_I) \qquad (14)$$

The silicone rubber capillaries are homogeneous, and unlike the CA fibers, one need not use the specific permeability here. However, the term (Q/d) is still used in Eq. 12 for the sake of uniformity. The quantity d here is known, however, and is equal to $(r_O - r_I)$, i.e., the capillary thickness in unstressed condition.

Note also that y_{2j}, and not y'_{2j}, is used on the righthand side of Eq. 12 since silicone rubber is homogeneous.

Let us now define a new quantity, R_A, as:

$$R_A = (\pi D_{lmS} N_{TS} l_e)/(\pi D_{OCA} N_{TCA} l_e)$$

or,
$$R_A = D_{lmS} N_{TS}/(D_{OCA} N_{TCA}) \quad (15)$$

The quantity R_A is the ratio of the total effective permeation area of the silicone rubber capillaries to that of the CA hollow fibers. It is an important parameter in the analysis of a two-membrane permeator. Note that the effective length of each kind of fiber is the same. Equation 12 is made dimensionless by using Eqs. 3–7 and Eq. 15:

$$d(V_2^* y_{2j})/dl^* = gR_A K C_{2j}(x_j - \gamma_2 y_{2j}), \quad j = 1, 2, 3 \quad (16)$$

Writing Eq. 16 for $j = 1$, 2, and 3, and adding up, one gets

$$dV_2^*/dl^* = gR_A K(B_2 - \gamma_2 E_2) \quad (17)$$

where

$$B_2 = C_{21}x_1 + C_{22}x_2 + C_{23}x_3 = C_{23} + (C_{21} - C_{23})x_1 + (C_{22} - C_{23})x_2 \quad (18)$$

$$E_2 = C_{21}y_{21} + C_{22}y_{22} + C_{23}y_{23} = C_{23} + (C_{21} - C_{23})y_{21} + (C_{22} - C_{23})y_{22} \quad (19)$$

From a material balance on component j on the feed side,

$$d(L^* x_j)/dl^* = d(V_1^* y_{1j})/dl^* + d(V_2^* y_{2j})/dl^* = KC_{1j}(x_j - \gamma_1 y'_{1j}) + gR_A K C_{2j}(x_j - \gamma_2 y_{2j}) \quad j = 1, 2, 3 \quad (20)$$

where

$$L^* = L/L_f \quad (21)$$

Substituting $j = 1$, 2, and 3 in Eq. 20, and adding up,

$$dL^*/dl^* = K(B_1 - \gamma_1 E_1) + gR_A K(B_2 - \gamma_2 E_2) \quad (22)$$

Using the following two identities

$$dx_j/dl^* = [d(L^* x_j)/dl^* - x_j(dL^*/dl^*)]/L^* \quad (23)$$

$$dy_{ij}/dl^* = [d(V_i^* y_{ij})/dl^* - y_{ij}(dV_i^*/dl^*)]/V_i^* \quad (24)$$

the following equations can be developed from Eqs. 2, 8, 16, 17, 20, and 22:

$$dx_1/dl^* = K[x_1(C_{11} - B_1) - \gamma_1(C_{11}y'_{11} - x_1 E_1) + gR_A x_1(C_{21} - B_2) - gR_A \gamma_2(C_{21}y_{21} - x_1 E_2)]/L^* \quad (25)$$

$$dx_2/dl^* = K[x_2(C_{12} - B_1) - \gamma_1(C_{12}y'_{12} - x_2 E_1) + gR_A x_2(C_{22} - B_2) - gR_A \gamma_2(C_{22}y_{22} - x_2 E_2)]/L^* \quad (26)$$

$$dy_{11}/dl^* = K[C_{11}x_1 - y_{11}B_1 - \gamma_1(C_{11}y'_{11} - y_{11}E_1)]/V_1^* \quad (27)$$

$$dy_{12}/dl^* = K[C_{12}x_2 - y_{12}B_1 - \gamma_1(C_{12}y'_{12} - y_{12}E_1)]/V_1^* \quad (28)$$

$$dy_{21}/dl^* = gR_A K[C_{21}x_1 - y_{21}B_2 - \gamma_2 y_{21}(C_{21} - E_2)]/V_2^* \quad (29)$$

$$dy_{22}/dl^* = gR_A K[C_{22}x_2 - y_{22}B_2 - \gamma_2 y_{22}(C_{22} - E_2)]/V_2^* \quad (30)$$

The pressure ratios γ_1 and γ_2 are also functions of fiber length. The derivative of γ_1 (the CA side) can be obtained following Pan and Habgood (1978) and Pan (1983):

$$d\gamma_1/dl^* = -K_{CA} V_1^*/\gamma_1 \quad (31)$$

where

$$K_{CA} = 128\,\mu_{CA} R_g T l_e L_f/(\pi D_{ICA}^4 N_{TCA} P_f^2) \quad (32)$$

The derivative of γ_2 is much more complicated owing to the fact that the capillary radii change upon pressurization. Utilizing the developments by Thorman and Hwang (1978) it can be shown that

$$\frac{d\gamma_2}{dl^*} = \left(\frac{\lambda_1}{\lambda_2} + 8.0\right) K_{S1} \frac{V_2^*}{\gamma_2} + \frac{1}{K_{S2} V_2^*/\gamma_2 - (1/8\,K_{S1})(\gamma_2/V_2^*)} \quad (33)$$

where

$$K_{S1} = R_g T \mu_S l_e L_f/(\pi R_1^4 N_{TS} P_f^2) \quad (34)$$

and

$$K_{S2} = L_f M_{w,avg}/(6\pi l_e \mu_S N_{TS}) \quad (35)$$

The gas mixture viscosities μ_{CA} and μ_S in Eqs. 31 and 33 are functions of composition, and are evaluated using models described in section 9-5 of Reid et al. (1977). The details are given in Sengupta (1985).

The terms λ_1 and λ_2 used in Eq. 33 are given as (Thorman and Hwang, 1978):

$$\lambda_1 = 8(-1.0 - 0.75\,Re_w + 0.0407\,Re_w^2) \quad (36)$$

$$\lambda_2 = 1.0 - 0.056\,Re_w + 0.0154\,Re_w^2) \quad (37)$$

where Re_w, the local wall Reynolds number for permeation can be shown in this case to be (Sengupta, 1985):

$$Re_w = L_f[V_2^*(M_{w1} - M_{w3})dy_{21}/dl^* + V_2^*(M_{w2} - M_{w3})dy_{22}/dl^* + M_{w,avg}dV_2^*/dl^*]/(2\pi l_e \mu_S N_{TS}) \quad (38)$$

The term $M_{w,avg}$ used in Eqs. 35 and 38 is given by

$$M_{w,avg} = \sum_{j=1}^{3} y_{2j} M_{wj} \quad (39)$$

For the countercurrent flow pattern, one has to solve a set of eleven differential equations, i.e., Eqs. 8, 17, 22, 25–31, and 33, involving six compositions: x_1, x_2, y_{11}, y_{12}, y_{21}, y_{22}; three flow rates: V_1^*, V_2^*, and L^*; and two pressure ratios: γ_1, γ_2. This is a split boundary value problem, and the equations are solved subject to the boundary conditions:

$$\text{at} \quad l^* = 0, \quad V_1^* = 0; \quad V_2^* = 0;$$
$$y_{ij} = y'_{ij}(\gamma_i, x_j); \quad i = 1, 2; \quad j = 1, 2 \tag{40}$$

$$\text{at} \quad l^* = 1, \quad L^* = 1; \quad x_1 = x_{f1}; \quad x_2 = x_{f2};$$
$$\gamma_1 = (\gamma_{o1}^2 + 2K_{CA}V_1^* l_{pCA}/l_e)^{1/2};$$
$$\gamma_2 = (\gamma_{o2}^2 + 16K_{S1}V_2^* l_{pS}/l_e)^{1/2}; \tag{41}$$

Here γ_{o1} and γ_{o2} are open-end permeate pressure ratios:

$$\gamma_{o1} = p_{oCA}/P_f; \quad \gamma_{o2} = p_{oS}/P_f \tag{42}$$

To calculate some of the constants in the above set of equations, one needs to know the actual dimensions (upon deformation) of the silicone rubber capillaries, R_O and R_I, at each location in the permeator. This is done by carrying out a deformation analysis following Stern et al. (1977). From known capillary dimensions in unstressed condition (r_O and r_I) one can calculate R_O and R_I at any location inside the permeator for given values of pressures inside and outside the capillary, if the Young's modulus for silicone rubber is known (Sengupta, 1985).

Some of the key steps in the solution process are highlighted below.

1. Supply the permeator constants, i.e., D_{ICA}, D_{OCA}, r_I, r_O, l_e, N_{TCA}, N_{TS}, l_{pCA}, l_{pS}, and T.
2. Supply the system parameters, i.e., $(Q/d)_{ij} - s$, pure-component viscosities, species molecular weights, Young's modulus for silicone rubber, etc.
3. Supply the values of the operating variables, i.e., L_f, P_f, p_{oCA}, p_{oS}, feed compositions x_{f1} and x_{f2}.
4. Calculate D_{lmS}, $C_{ij} - s$, K, R_A, γ_{o1}, γ_{o2}.
5. Solve the system of differential equations. As part of this process, one has to compute in each step the following quantities:
   a. R_I, R_O, and g; from a deformation analysis
   b. μ_{CA} and μ_S
   c. $M_{w,avg}$, Re_w, λ_1, λ_2, K_{CA}, K_{S1}, and K_{S2}

All numerical calculations were carried out on a DEC 10 mainframe computer. Standard IMSL subroutines were used whenever possible. To extract the species permeability values from the data of pure-component permeation experiments, a parameter estimation technique (Lee, 1968) was employed. The details are given in Sengupta (1985). To solve the actual boundary value problem, IMSL routine DVCPR, which is based on a finite-difference algorithm, was used. Initial estimates of the values of the variables had to be generated for this process. This was down by solving the given differential equations assuming cocurrent flow and no pressure drop (an initial value problem).

Once the system of equations are solved subject to the prescribed tolerance, results are obtained in terms of the following quantities:

1. The values of x_1 and x_2 at $l^* = 0$. These indicate the composition in the reject stream.
2. The values of V_1^* and V_2^* at $l^* = 1$. These give the stage permeate cuts. There are two permeate cuts here, θ_{CA} and θ_S, defined as

$$\theta_{CA} = V_1^*(\text{at } l^* = 1); \quad \theta_S = V_2^*(\text{at } l^* = 1) \tag{43}$$

3. The values of y_{11}, y_{12}, y_{21}, and y_{22} at $l^* = 1$. These indicate the permeate compositions at the permeate outlets.
4. The values of γ_1 and γ_2 at $l^* = 0$. These indicate the extents of permeate pressure buildups at the closed ends of the two permeate streams.

After these values are calculated, they can be compared directly with the corresponding experimental results.

So far we have discussed only the countercurrent flow pattern. For cocurrent flow the basic analysis remains essentially the same. However, one can express L^* here in terms of V_1^* and V_2^* through the material balance:

$$L^* = 1 - V_1^* - V_2^* \tag{44}$$

Therefore one deals with a system of ten differential equations. The boundary conditions are altered accordingly.

Results and Discussion

In this section the pure-component permeability data are presented first. The separation results in terms of both experiments and simulation are considered next. The effect of a few important parameters on ternary separation in the two-membrane configuration are explored. Some of the results shown here are derived from both experiment and simulation. However, in situations where experimental data are not available, or where it was not feasible to carry out experiments, only the simulation results are presented.

Experimentally obtained specific permeabilities of He, CO_2, and N_2 are plotted in Figures 5 and 6, for CA and silicone rubber membrane, respectively, against the feed pressure of the pure species considered. The plots indicate that the specific permeabilities of the three species are practically constant, for each

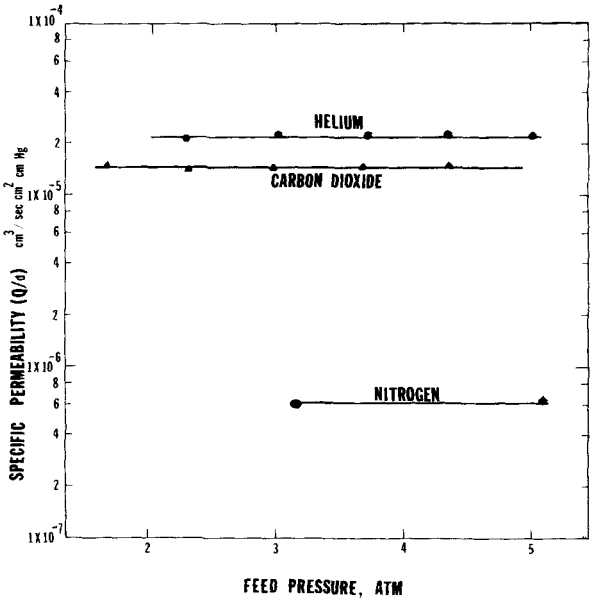

Figure 5. Specific permeabilities through CA membrane.

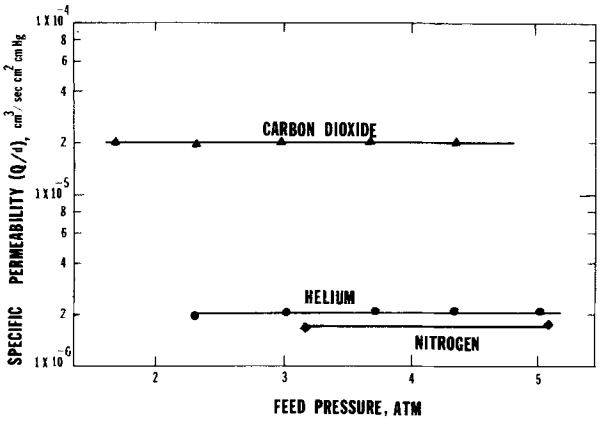

Figure 6. Specific permeabilities through silicone membrane.

of the two membranes, over the pressure range studied. In subsequent simulations an average specific permeability value is utilized for each species-membrane combination (a total of six). The N_2 permeability through silicone rubber as reported here is very close to that reported by Stern et al. (1977), and the selectivities (the ratio of the permeabilities of any two species) are similar to those determined by Robb (1965). For CA membrane also, the selectivities are in the expected range (as given in Sengupta and Sirkar, 1984), and the actual specific permeability values are similar to those reported in Perrin and Stern (1985b). However, these values are about one order of magnitude lower than those reported in, for example, Pan et al. (1978). This is presumably because the membrane structure and the effective membrane thickness in that study are different from those in the present case.

Before the results for the two-membrane permeator are presented, some results on the separation through CA membrane alone are shown in Figure 7. For a CA membrane permeator, the separation data in terms of stage cut (defined as the fraction of the feed taken out as permeate) and the reject and permeate mole fraction of the most permeable species, helium, are compared with the corresponding values predicted by the simulation. The simulation was done twice: once assuming that the CA membrane is asymmetric in structure, and a second time assuming that it is symmetric. The purpose of the above comparison is twofold. First, the plot compares the experimental separation data with the simulation (which uses the pure-component permeabilities shown already). Thus one can check whether the pure-component permeabilities can be used directly in modeling separations. Second, by comparing the predictions from an asymmetric membrane model with those from a symmetric membrane model, this plot indicates the effect of the model on simulation results.

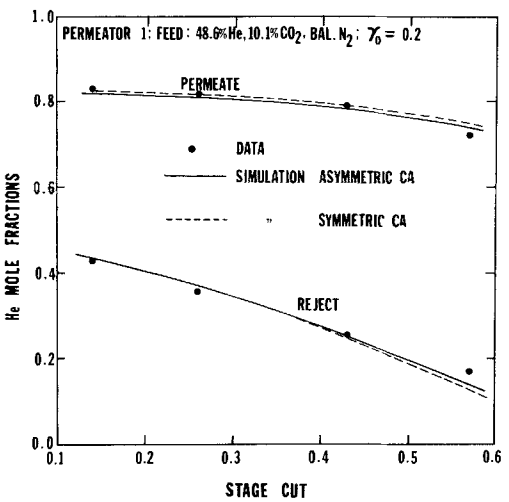

Figure 7. Separation through CA membrane only, experiment vs. simulation.

Figure 7 shows that the data and simulation results are sufficiently close. Therefore, pure-component permeabilities can be used in separation models. However, the differences between the predictions from the two models are not large enough to let one conclude unequivocally which model would better fit the data. It can also be said that under the chosen experimental conditions the choice of a model is not going to affect the results significantly, and the basic behavior or performance of the CA membrane as predicted from simulation will remain unaltered irrespective of the model utilized in simulation.

An aspect of general importance here is the pressure drop in the lumen of the fibers. Such pressure drop data are shown in Table 3 for pure-component permeation runs as well as separation runs. The tabulated data indicate that the lumen pressure buildup is truly significant for CA hollow fibers, with the permeate pressure inside the lumen varying in some cases by almost 50% from the closed end to the open end of the fiber. This is since the inside diameter of the CA fibers is very small. The need to include Eq. 31 in the model is thus demonstrated. It should be noted that the simulation has predicted the $\Delta P - s$ quite well, even though that particular comparison is not shown here. The pressure drop in the silicone rubber capillaries, on the other hand, is almost always insignificant, since their bores are

Table 3. Samples of Lumen Pressure Drop Data*

Pure-Component Permeation				
Membrane	Gas	Feed Press. atm	Permeation Rate cm^3/min	Max. Lumen Press. Drop atm
CA	He	5.0	70.7	0.9
		2.3	21.7	0.4
	CO_2	4.3	42.6	0.5
		1.7	8.7	0.2
S	He	5.0	12.6	0.0
		2.3	4.5	0.0
	CO_2	4.3	104.6	0.03
		1.7	25.3	0.0

Separation in Two-membrane Permeator				
Feed Press. atm	CA Permeate Rate cm^3/min	S Permeate Rate cm^3/min	Max. Lumen Press. Drop, atm	
			CA	S
5.1	16.9	16.2	0.3	0.02
5.0	6.7	12.4	0.2	0.02
10.0	63.3	13.0	0.9	**
9 9	24.1	11.3	0.5	**

*At the fiber open ends the pressure is always atmospheric
**Silicone capillaries collapse mechanically; their closed end pressure is beyond the pressure gauge range (>60 psig, 420 kPa)

much more open, and the total permeation rates are mostly low. The mechanical deformation of the capillaries as computed by the model is significant, however, even though not reported in the table. Also, when operated at high feed pressures ($\gamma_o \simeq 0.1$), the table demonstrates complete mechanical collapse of the rubber capillaries, resulting in pressure values at the closed capillary ends that are too high.

Next we consider ternary separation in a two-membrane permeator. The experimental separation data for the cocurrent flow pattern are compared with the simulation in Figure 8. Since helium is the most permeable through CA, and CO_2 is the most permeable through silicone, the mole fraction of He in CA permeate, $y_{CA,He}$, is plotted against the CA permeate stage cut θ_{CA}, while the mole fraction of CO_2 in the S permeate, y_{S,CO_2}, is plotted against the S permeate stage cut θ_S. Besides, the mole fractions of He and N_2 in the reject stream, $x_{o,He}$ and x_{o,N_2}, are also plotted here against the stage cut θ_{CA}. The quantity $x_{o,He}$ indicates the extent to which helium is recovered from the feed, while x_{o,N_2} indicates the extent of purification of N_2. As Figure 8 shows, the data and the simulation are sufficiently close except at very high stage cut values. The model thus predicts the permeator performances over a wide range.

Figure 8 actually shows the results of two simulations, one where the CA membrane is assumed to be asymmetric, and another where it is assumed to be symmetric. The figure demonstrates that the two models predict identical values over most of the stage cut range, implying that the presence of a second membrane (silicone) in the two-membrane permeator attenuates substantially the effect of the model chosen for CA membrane structure.

Two more observations can be made from Figure 8. Note first that the $y_{CA,He}$ vs. θ_{CA} curve is practically flat for most of the stage cut range. In single-membrane permeators, the permeate mole fraction almost always decreases with increasing stage cut (Blaisdell and Kammermeyer, 1973). In the present case, the permeabilities of He and CO_2 through CA are not too different, and so they compete with each other in permeation. However, silicone membrane, which is comparatively much more selective to CO_2 than CA is to He, takes out a substantial amount of CO_2 from the feed. So the mole fraction of He in the feed channel decreases much less rapidly than usual, a phenomenon that translates itself into the almost constant value of $y_{CA,He}$. On the other hand, the y_{S,CO_2} vs. θ_S curve is not flat because He—CO_2 selectivity through CA is very low. The shapes of the curves for $x_{o,He}$ and x_{o,N_2} are as expected, indicating that with higher stage cut the feed gets stripped of helium, and is more enriched in N_2.

A second point to consider is the significant deviation of the data from simulation at high stage cut values. This phenomenon has been observed under all parametric conditions in the present work. It is believed that the assumption of plug flow on the shell side, and the assumption of negligible concentration gradients in the gas phases, may not be valid for very low feed flow rate conditions (necessary to attain high stage cuts in the present case, as the permeation areas are constant). That is why the simulations do not match well with the data at high stage cuts.

Figure 9 compares the performances of a two-membrane permeator operated in two different modes, cocurrent and countercurrent. Both simulation and data are presented. Although the data and simulation do not match well for the quantity y_{S,CO_2} in countercurrent mode, the simulations and other data indicate that the permeator performs better in countercurrent mode than in cocurrent mode. This should indeed be the case if one considers the two-membrane permeator to be equivalent to a combination of two single-membrane permeators integrated locally, since for the latter, countercurrent flow is almost always better (Walawender and Stern, 1972; Pan and Habgood, 1974; Antonson et al., 1977; Sengupta and Sirkar, 1984).

The effect of an important parameter, R_A, the membrane area ratio, is explored next in Figure 10, where the performance of permeator no. 1 ($R_A \sim 1$) is compared to that of permeator no. 2 ($R_A \sim 2$). As Table 2 shows, an increase in R_A in this case means a decrease in CA membrane area, with the silicone rubber membrane area remaining same. Figure 10 indicates that an increase in R_A improves the enrichments (permeate mole fractions) and recoveries (reject mole fractions). The explanation is as follows. Since the permeabilities of He and CO_2 through CA are similar, and since in the feed inlet He concentration is about five times that of CO_2, a decrease in CA area means that comparatively less CO_2 is allowed to come into the CA permeate. As

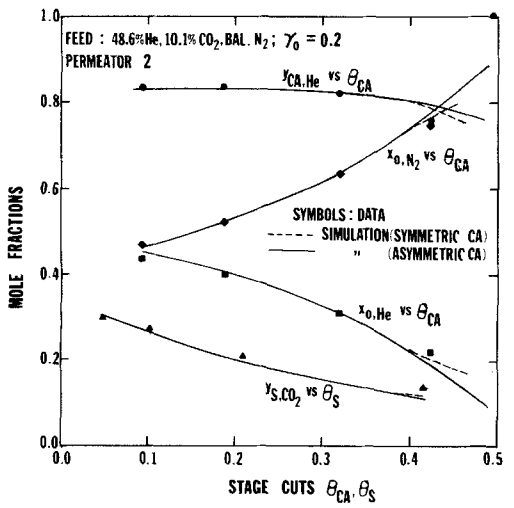

Figure 8. Separation in two-membrane permeator, experiment vs. simulation.

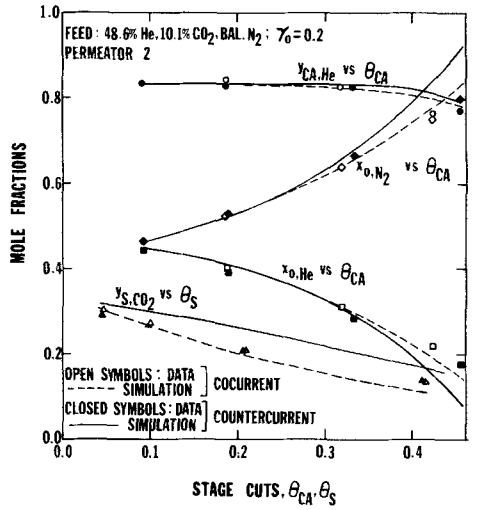

Figure 9. Effect of flow pattern in two-membrane permeator.

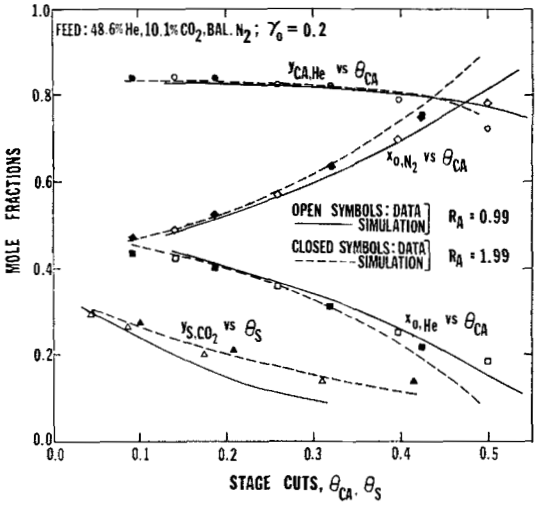

Figure 10. Effect of membrane area ratio in two-membrane permeator.

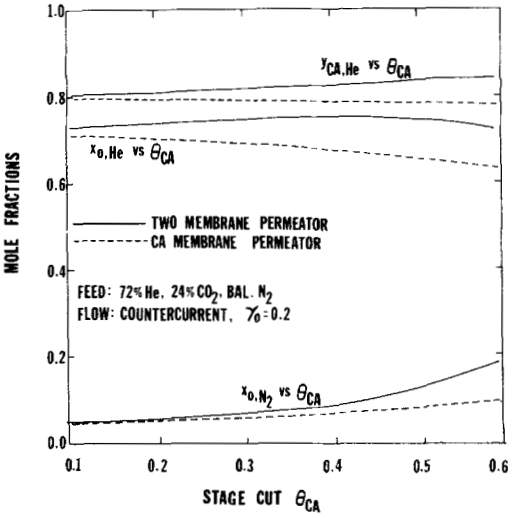

Figure 12. Two-membrane permeator vs. CA membrane permeator for feed with low N_2 content. Simulation only.

a result, the CO_2 mole fraction in the feed channel would be higher, and this is magnified in the silicone permeate since silicone rubber is much more selective to CO_2 than to He and N_2.

So far we have studied single-membrane and two-membrane permeators separately. A comparison between these two under identical conditions should be of interest also. For example, one may compare the behavior of the CA membrane permeate and the reject in a two-membrane permeator with the corresponding behavior in a permeator containing only CA membrane. This would in fact indicate the advantages of the two-membrane permeator, if any.

Since the two-membrane permeator contains membranes with opposing selectivities, its performance is expected to be influenced significantly by the feed composition. Consider two cases. First, the ternary feed into the permeator contains a substantial quantity of the slowest permeating species, N_2. In the second case, the feed contains very little N_2, but the relative concentrations of He and CO_2 on an N_2-free basis are same in both the cases. One can expect that the effect of the reverse selectivities will be attenuated by the presence of N_2, and thus as one goes from a high N_2 feed to a low N_2 feed (approaching a binary system of He and CO_2) the effects of the two-membrane configuration should be more pronounced.

Figures 11 and 12 compare a two-membrane permeator with a CA membrane permeator for different inlet feed compositions. The He to CO_2 molar ratio is same in both plots. For clarity, only simulation results are presented here. Both figures indicate that the two-membrane scheme yields richer permeate composition and more favorable reject composition (less He, more N_2) than the single-membrane separator. These facts demonstrate the basic underlying advantages of the two-membrane scheme. The plots also bear out the contention that as one approaches a near-binary system of He—CO_2, as in Figure 12, these advantages become more pronounced.

We return now to the study of parametric effects in a two-membrane permeator. Figure 13 shows the effect of the feed

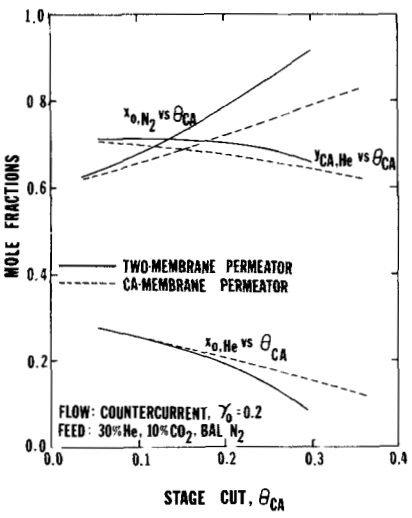

Figure 11. Two-membrane permeator vs. CA membrane permeator for feed with high N_2 content. Simulation only.

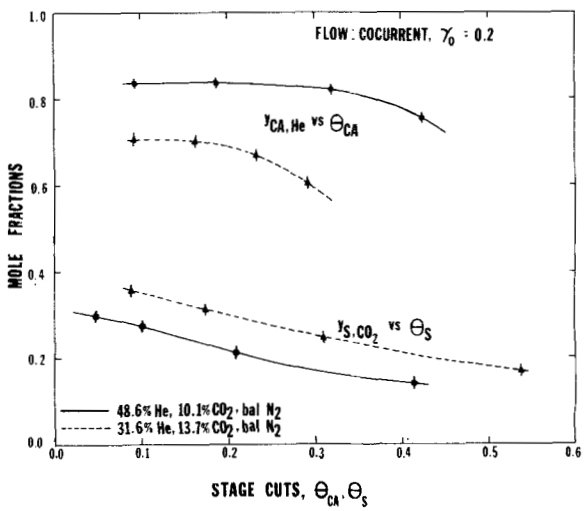

Figure 13. Feed composition effect on two-membrane permeator: experimental data.

composition on the experimentally observed permeator performance. Only a slight increase in the inlet CO_2 mole fraction in the feed gives a much higher value of y_{S,CO_2}, whereas a decrease in the feed He mole fraction combined with the increase in CO_2 mole fraction results in a drastic reduction in $y_{CA,He}$.

In the next plot, Figure 14, performances for two different permeate pressure ratio values of $\gamma_o \sim 0.1$ and $\gamma_o \sim 0.2$ are compared. Only simulation results are shown since at the higher feed pressure ($\gamma_o \sim 0.1$) the silicone rubber capillaries underwent drastic compression, preventing the acquiring of any meaningful experimental data. In general, a decrease in γ_o always improves the absolute values of the permeation rates, but the separation still depends on the membrane selectivity. Here the plot indicates that since CA is not very selective between He and CO_2, a decrease in γ_o does not increase $y_{CA,He}$ much. On the other hand, for silicone rubber at low stage cuts, the effect is more pronounced. At a high stage cut, the silicone permeate quality decreases because the deleterious effect of the elastic deformation of the silicone capillaries at high feed pressure nearly offsets the advantage of high feed pressure in terms of permeation.

In the last two plots, Figures 15 and 16, the effects of membrane selectivities on permeator performance are explored. Since the actual membrane permeabilities cannot be changed, comparisons can be done only with simulation results. However, such comparisons are quite useful in understanding the two-membrane permeator. Figure 15 compares the performance of an actual permeator with that of a hypothetical permeator where the CO_2 permeability through CA is one-tenth that of He. All five other permeabilities are the same as in the actual permeator. The purpose here is to find out what happens if the He—CO_2 selectivity through CA improves and comes up to the same level as the CO_2—He selectivity through silicone rubber. It is interesting to note that a decrease in $(Q/d)_{CA,CO_2}$ improves the overall separator performance in all respects. As less CO_2 is allowed in the CA permeate, $y_{CA,He}$ increases. This gives rise to higher CO_2 concentration in the feed channel, and in turn to higher values of y_{S,CO_2}. These facts again underline the basic locally-coupled feature of the two-membrane scheme, so that a change in the selectivity of one membrane affects the performance of not only that membrane, but that of the other also.

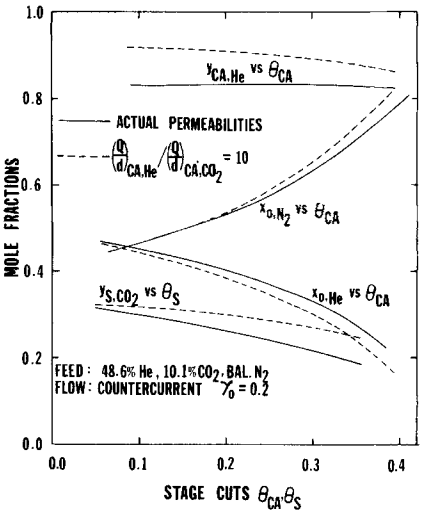

Figure 15. Effect of improved CA selectivity on two-membrane permeator: simulation only.

Similar results are shown in Figure 16. Here the actual permeator performance is compared with that of another which has a higher value of $(Q/d)_{S,He}$ such that CO_2—He selectivity through silicone rubber comes down to 1.5, which is about equal to the He—CO_2 selectivity through CA. It can be seen that the performance of the latter is very poor. This plot shows, vis a vis Figure 15, how a loss of selectivity by one membrane can significantly undermine the overall performance although it is actually accompanied by an improvement in one of the permeabilities.

Conclusion

A two-membrane permeator of the present configuration can achieve ternary separation in a single stage. This type of a separation scheme can be viewed as a combination of two separation processes with reverse selectivities that are coupled together locally, and that operate in parallel. The performance of any membrane would improve when a second membrane with the right kind of selectivity was brought together with the first

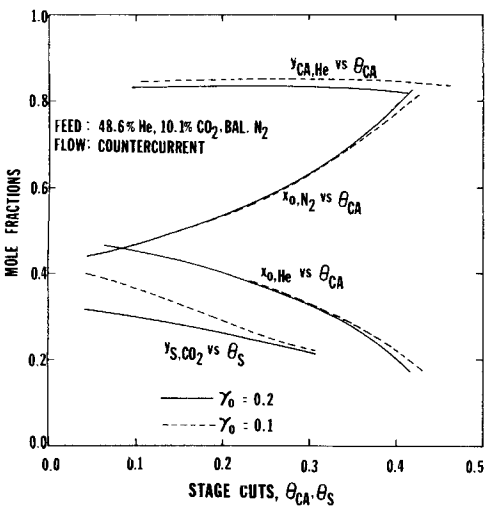

Figure 14. Pressure ratio effect on two-membrane permeator: simulation only.

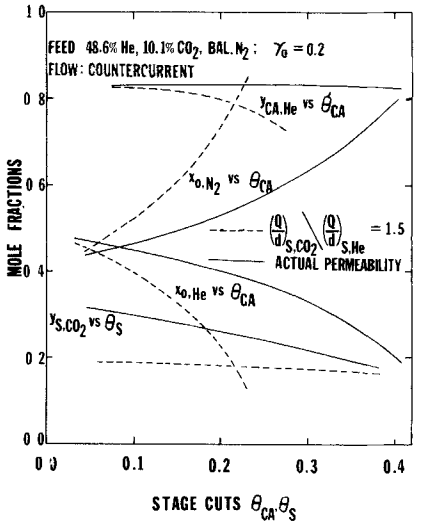

Figure 16. Effect of reduced S selectivity on two-membrane permeator: simulation only.

membrane in the present configuration. The improvement in performance is most pronounced when the ternary feed has the least amount of the slowest permeating component.

The two-membrane scheme operates better in countercurrent mode than in cocurrent mode. An increase in the relative permeation area of the membrane that is the more selective of the two improves the performance of both membranes. The effect of an increase in the feed pressure or a decrease in γ_o is more marked for the more selective membrane. An increase in the selectivity of one membrane improves the performance of both membranes in the permeator, and a decrease in the selectivity of one membrane undermines the performance of both.

Notation

B_1, B_2 = functions, Eqs. 9, 18
C_{ij} = normalized specific permeabilities in two-membrane permeator, Eq. 6
D_{ICA}, D_{OCA} = inside and outside diameters of cellulose acetate fibers, m
D_{lmS} = logarithmic mean of inside and outside diameters (unstressed values) of silicone capillaries, Eq. 14, m
E_1, E_2 = functions, Eqs. 10, 19
g = factor, Eq. 13, used to depict effect of elastic deformation in permeation equation for silicone rubber capillaries
K = constant, Eq. 7, used in simulation of two-membrane permeator
K_{CA} = constant, Eq. 32, used in pressure drop equation for CA permeate
K_{S1}, K_{S2} = constants, Eqs. 34, 35, used in pressure drop equation for S permeate
l = distance of any permeator location from closed end of fiber (independent variable)
l_e = total effective length of permeation in a permeator, m
l_{PCA} = potted length of CA fibers, m
l_{PS} = potted length of silicone rubber capillaries, m
l^* = dimensionless distance, Eq. 3
L = local feed flow rate at any permeator location, mol/s
L_f = feed flow rate at permeator entry, mol/s
L^* = dimensionless local feed flow rate, Eq. 21
M_{wi} = molecular weight of ith species, kg/mol
$M_{w,avg}$ = average molecular weight of a gas mixture, Eq. 39, kg/mol
N_{TCA}, N_{TS} = total number of CA fibers and silicone rubber capillaries, respectively, in permeator
p_1, p_2 = local permeate pressures in the two kinds of fibers in case of two-membrane permeator, Pa
p_{oCA}, p_{oS} = permeate pressures at open ends of CA fibers and silicone capillaries, Pa
P_f = feed channel pressure, Pa
Q/d = specific permeability of a gas species, mol/s · m² · Pa
$(Q/d)_{ij}$ = value of (Q/d) through ith membrane of jth species, for two-membrane permeator
r_I, r_O = inside and outside radii of silicone capillaries prior to elastic deformation, m
R_I, R_O = inside and outside radii of silicone capillaries, actual values, upon elastic deformation, m
R_A = ratio of total silicone membrane area to total cellulose acetate membrane area, Eq. 15
R_G = universal gas constant, Pa · m³/mol · K.
Re_w = wall Reynolds number, Eq. 38
T = absolute temperature, K.
V_1, V_2 = local total permeate flow rates in the two kinds of fibers, mol/s
V_1^*, V_2^* = normalized values of V_1 and V_2, Eq. 4
x_{fi} = mole fraction of ith component at feed entry
x_{oi} = mole fraction of ith component in permeator outlet
y_{ij} = local mole fraction in permeate from ith membrane, of jth component
y'_{ij} = permeate mole fraction based on local cross flow, Eq. 11

Greek letters

α_{ij} = selectivity of a membrane between species i and j, $= (Q/d)_i/(Q/d)_j$
γ_1, γ_2 = pressure ratios in case of two-membrane permeators, Eq. 5
γ_{oi} = value of γ_i at permeate outlet, Eq. 42
λ_1, λ_2 = functions, Eqs. 36, 37
μ_{CA}, μ_S = local viscosities of CA permeate and S permeate
θ_{CA}, θ_S = stage cuts defined in Eq. 43.

Literature cited

Antonson, C. R., R. J. Gardner, C. F. King, and D. Y. Ko, "Analysis of Gas Separation by Permeation in Hollow Fibers," *Ind. Eng. Chem. Process Des. Dev.*, **16,** 463 (1977).

Blaisdell, C. T., and K. Kammermeyer, "Countercurrent and Cocurrent Gas Separation," *Chem. Eng. Sci.*, **28,** 1249 (1973).

Chern, R. T., W. J. Koros, and P. F. Fedkiw, "Simulation of a Hollow-Fiber Gas Separator: The Effects of Process and Design Variables," *Ind. Eng. Chem. Process Des. Dev.*, **24,** 1015 (1985).

Kimura, S., T. Nomura, T. Miyauchi, and M. Ohno, "Separation of Rare Gases by Membranes," *Radiochem. Radioanal. Lett.*, **13,** 349 (1973).

Lee, E. S., *Parameter Estimation and Invariant Imbedding,* Academic Press, New York, London (1968).

MacDonald, W., and C. Y. Pan, Method for Drying Water-wet Membranes, United States Patent No. 3,842,515 (Oct. 22, 1974).

Ohno, M., O. Ozaki, H. Sato, S. Kimura, and T. Miyauchi, "Radioactive Rare Gas Separation Using a Separation Cell with Two Kinds of Membrane Differing in Gas Permeability Tendency," *J. Nuclear Sci. Technol.*, **14,** 589 (1977).

Pan, C. Y., "Gas-separation by Permeators with high-flux Asymmetric Membranes," *AIChE J.*, **29,** 545 (1983).

Pan, C. Y., and H. W. Habgood, "An Analysis of the Single-Stage Gaseous Permeation Process," *Ind. Eng. Chem. Fundam.*, **13,** 323 (1974).

———, "Gas-separation by Permeation. II: Effect of Permeate Pressure Drop and Choice of Permeate Pressure," *Canad. J. Chem. Eng.*, **56,** 210 (1978).

Pan, C. Y., C. D. Jensen, C. Bielech, and H. W. Habgood, "Permeation of Water Vapor through Cellulose Triacetate Membranes in Hollow-Fiber Form," *J. Appl. Polymer Sci.*, **22,** 2307 (1978).

Perrin, J. E., and S. A. Stern, "Modeling of Permeators with Two Different Types of Polymer Membranes," *AIChE J.*, **31,** 1167 (1985a).

———, "Separation of a Helium-Methane Mixture in Permeators with Two Different Types of Polymer Membranes," *AIChE J.*, **32,** 1,889 (1985b).

Reid, R. C., J. M. Prausnitz, and T. K. Sherwood, *The Properties of Gases and Liquids,* 3rd ed., McGraw-Hill, New York (1977).

Robb, W. L., "Thin Silicone Membranes—Their Properties and Some Applications," Rept. No. 65-C-031, R&D Center, General Electric Co., Schenectady, NY (1965).

Sengupta, A., Ph.D. Diss. "Investigation on Binary and Ternary Gas Separations Using Polymeric Membrane Permeators," Stevens Inst. Technol., Hoboken, NJ (1985).

Sengupta, A., and K. K. Sirkar, "Multicomponent Gas Separation by an Asymmetric Permeator Containing Two Different Membranes," *J. Membrane Sci.*, **21,** 73 (1984).

Sirkar, K. K., (1977), "Separation of Gaseous Mixtures with Asymmetric Dense Polymeric Membranes," *Chem. Eng. Sci.*, **32,** 1137 (1977).

———, "Asymmetric Permeator—A Conceptual Study," *Separ. Sci. Technol.*, **15,** 1091 (1980).

Stern, S. A., S. K. Sen, and A. K. Rao, "The Permeation of Gases Through Symmetric and Asymmetric (Loeb-type) Cellulose Acetate Membranes," *J. Macromol. Sci. Phys.*, **B10**(3), 507 (1974).

Stern, S. A., F. J. Onorato, and C. Libove, "The Permeation of Gases Through Hollow Silicone Rubber Fibers: Effect of Fiber Elasticity on Gas Permeability," *AIChE J.*, **23,** 567 (1977).

Stern, S. A., J. E. Perrin, and E. J. Naimon, "Recycle and Multimembrane Permeators for Gas Separations," *J. Membrane Sci.*, **20,** 25 (1984).

Thorman, J. M., and S. T. Hwang, "Compressible Flow in Permeable Capillaries Under Deformation," *Chem. Eng. Sci.*, **33,** 15 (1978).

Walawender, W. P., and S. A. Stern, "Analysis of Membrane Separation Parameters. II: Countercurrent and Cocurrent Flow in a Single Permeation Stage," *Separ. Sci.*, **7,** 553 (1972).

Manuscript received Mar. 7, 1986, and revision received Oct. 9, 1986.